

## Accepted Article

**Title:** Breakdown of Curly Arrow Rules in Anthraquinone

**Authors:** Jehan Alqahtani, Hatef Sadeghi, Sara Sangtarash, and Colin J Lambert

This manuscript has been accepted after peer review and appears as an Accepted Article online prior to editing, proofing, and formal publication of the final Version of Record (VoR). This work is currently citable by using the Digital Object Identifier (DOI) given below. The VoR will be published online in Early View as soon as possible and may be different to this Accepted Article as a result of editing. Readers should obtain the VoR from the journal website shown below when it is published to ensure accuracy of information. The authors are responsible for the content of this Accepted Article.

**To be cited as:** *Angew. Chem. Int. Ed.* 10.1002/anie.201807257  
*Angew. Chem.* 10.1002/ange.201807257

**Link to VoR:** <http://dx.doi.org/10.1002/anie.201807257>  
<http://dx.doi.org/10.1002/ange.201807257>

# Breakdown of Curly Arrow Rules in Anthraquinone

Jehan Alqahtani,<sup>[a]</sup> Hatf Sadeghi,<sup>\*[a]</sup> Sara Sangtarash,<sup>[a]</sup> Colin J. Lambert<sup>[a]</sup>

**Abstract:** Understanding and controlling quantum interference QI in single molecules is fundamental to the development of QI based single molecule electronics. Over the past decade, simple rules such as counting rules, curly arrow rules, circuit rules and more recently magic ratio rules have been developed to predict QI patterns in polycyclic aromatic hydrocarbons. These rules have been successful in explaining observed electronic transport properties of molecular junctions and provide helpful design tools for predicting properties of molecules before their synthesis. Curly arrow rules are widely used by chemists, material scientists and physicists to predict destructive QI. Here we examine the validity of curly arrow rules in fully conjugated anthracene and dihydroxyanthracene, cross-conjugated anthraquinone and broken conjugated dihydroanthracene attached to graphene or gold electrodes through pi-pi stacking or thiol and Au-C anchors. For the first time, we demonstrate that curly arrow rules break down in molecular junctions formed by cross-conjugated anthraquinone. In contrast with the destructive QI predicted by curly arrow rules for a meta connected anthraquinone core, we demonstrate that QI is constructive. This behavior is independent of the choice of electrode material or anchor groups. This is significant, because by changing the redox state of meta connected dihydroxyanthracene to form meta connected anthraquinone, the conductance of the junction increases by couple of orders of magnitude due to the cross over from constructive to destructive QI. This opens new avenues for realization of quantum interference based single molecule switches.

Single molecule electronics has recently witnessed significant progress<sup>[1]</sup>. Much attention has been drawn to phase coherent quantum interference (QI)<sup>[2]</sup>, which plays an essential role in electronic transport through single molecules<sup>[3]</sup>. Simple design rules such as counting rules<sup>[2c]</sup>, curly arrow rules<sup>[1c,4]</sup>, quantum circuit rules<sup>[5]</sup> and more recently magic ratio rules<sup>[6]</sup> have been developed to predict the effect of interference patterns in polycyclic aromatic hydrocarbons (PAHs). When a molecule is connected to metallic electrodes with different connectivities, electrons traversing multiple paths interfere constructively or destructively<sup>[7]</sup>. This constructive (destructive) QI leads to a high (low) conductance. The above rules are helpful in identifying if destructive or constructive QI is expected for a given connectivity. In addition, magic ratio rules provide information about ratios of conductances belonging to different constructive connectivities. These simple rules provide basic understanding of a molecular scale junctions and can qualitatively explain various experiments<sup>[1c,6a,c]</sup>.

Over the past decades, curly arrow rules (CARs) have been used to predict destructive QI in molecules<sup>[1c]</sup>. Curly arrows predict the movement of pairs of electrons<sup>[4]</sup>. When an electron is placed on a site

in a PAH, the charges should be balanced. A bond is broken if electrons are removed from it; otherwise a bond is formed if electrons are placed between two atoms. This process is illustrated by curly arrows. When an electron path was formed by moving pairs of electrons (using curly arrows) between two injection and collection connectivities, constructive QI is expected. Otherwise, if such a path was not found, destructive QI is predicted<sup>[1c,4]</sup>. For example for a *para* connected anthracene (AC1 in figure 1a), the arrows shows the path that the electron could take to travel through the molecule<sup>[1c]</sup>. In contrast, in *meta* connected anthracene (AC2 in figure 1b), a loop is formed and the electron entered to the molecule cannot exit<sup>[1c]</sup>. In this case, the CAR predicts destructive QI. Indeed these predictions for anthracene have been observed experimentally<sup>[3b]</sup>. In anthraquinone, when curly arrows are drawn, due to the presence of oxygen, there is no path between both *para* and *meta* connectivities and therefore, CARs predict destructive QI for both *meta* and *para* connectivities (AQ1 and AQ2 in figure 1c,d). However, this is not supported with our first principles calculations.

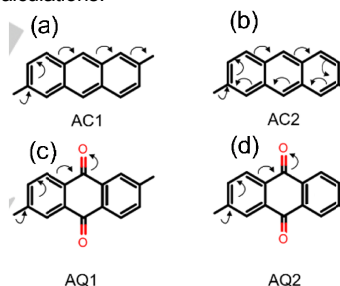


**Figure 1.** The curly arrow rule (CAR). (a) *para* and (b) *meta* connected conjugated anthracene labelled by AC1 and AC2, respectively. (c) *para* and (d) *meta* connected cross conjugated anthraquinone labelled by AQ1 and AQ2, respectively.

In this communication, we show that the curly arrow rule breaks down. We examine the validity of CARs using anthraquinone based molecular junctions. In contrast with curly arrow rules which predict destructive QI for both *para* (fig. 1c) and *meta* (fig. 1d) connected anthraquinone, we demonstrate destructive QI for *para* connected anthraquinone (fig. 1c), but constructive QI for *meta* connectivity. This is independent of the choice of anchor group or electrodes material. In contrast to conjugated anthracene, anthraquinone is a cross-conjugated molecule. If each oxygen in anthraquinone was replaced by two hydrogens, a broken conjugated dihydroanthracene is obtained. In what follows, we also investigate the quantum interference effect in these three types of molecules. We study the cross-conjugated anthraquinone molecular junctions (AQ1 and AQ2 in fig. 2) and compare it with its conjugated counterpart anthracene (AC1 and AC2 in fig. 2) and dihydroxyanthracene (QC1 and QC2 in fig. 2) and broken conjugated dihydroanthracene (AH)<sup>[8]</sup> (fig. S3 of the SI). Molecular junctions are formed by attaching these molecules to gold electrodes via thiol<sup>[9]</sup> (fig. 2a) and direct Au-C<sup>[10]</sup> (fig. 2b) bonds and to graphene electrodes through pi-pi stacking with pyrene anchors<sup>[11]</sup> (fig. 2c). We have constructed 22 different molecular junctions by combining ACs, Aqs, QCs and AHs with 2 electrodes and 3 anchors summarized in figures S1, S2 and S3 of the supporting information SI (See fig. S2 of the SI for details of molecular structure).

[a] J. Alqahtani, Dr. H. Sadeghi, Dr. S. Sangtarash, Prof. C.J. Lambert

Physics Department, Lancaster University,  
Lancaster LA1 4YB, UK  
Email: h.sadeghi@lancaster.ac.uk; c.lambert@lancaster.ac.uk

Supporting information for this article is given via a link at the end of the document

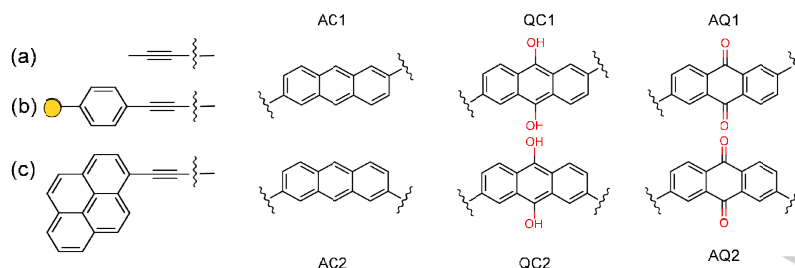


**Figure 2.** The structure of three systems with three central cores (AC, QC and AQ) via different connectivities. (a) A direct C-C bond with gold. (b) Thiol anchor with gold. (c) Pyrene with graphene.

In order to investigate the electronic properties of the junctions, we obtain the mean-field Hamiltonian of each structure from the optimized geometry of the junctions shown in figure S2 of the SI using density functional theory DFT<sup>[12]</sup> (see methods). We then combined these Hamiltonians with the transport code Gollum<sup>[13]</sup> to calculate the transmission coefficient  $T(E)$  of electrons with energy  $E$  passing from one electrode to the other. The conductance is proportional to  $T(E)$  via Landauer formula  $G=G_0T(E_F)$  where  $G_0$  is conductance quantum, and  $E_F$  is the Fermi energy of electrode (see methods).

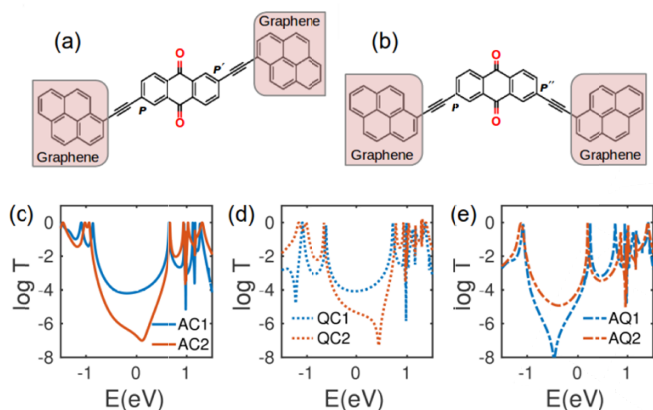


**Figure 3.** Transmission coefficients for electrons passing through the junctions with graphene electrodes via pyrene anchor groups. (a,b) example of junctions formed by AQ cores connected to the anchors from *para* and *meta* connectivities. Transmission coefficients for (c) AC1 and AC2, (d) QC1 and QC2 and (e) AQ1 and AQ2. The features around  $E=1\text{eV}$  are mainly due to the changes in the number open channels in graphene electrodes.

Figure 3 shows the calculated transmission coefficient for junctions with graphene electrodes. Figures 3a,b show examples of the junctions formed using graphene electrodes, where AQ's are connected from different connection points to two pyrene electrodes through acetylene linkers. Pyrene anchors are connected to the electrodes (shaded regions in figure 3a,b) through pi-pi interaction with the pi system of graphene. The molecular structures of the junctions formed with graphene electrodes and these 6 molecules are shown in figure S2 in the SI. Figure 3c shows the transmission coefficient for graphene junctions formed by AC cores. In agreement with previous theoretical<sup>[3b,14]</sup> and experimental studies<sup>[3b,14b,c]</sup>, the conductance of *para* connected AC1 (fig. 2) shows high conductance due to a constructive QI whereas a low conductance is obtained in AC2 due to a destructive QI (fig. 3c). Note that since the junction including leads and molecule is formed from carbon and hydrogen, a uniform charge distribution is expected. Therefore, the DFT Fermi energy lies close to

the middle of the HOMO-LUMO gap. Similar behavior is obtained in the graphene/QC's/graphene molecular junction (fig. 3d). The transmission spectrum of QC's is slightly shifted to the right (negative gate) compared to  $T(E)$  of AC's. This is due to a weak electrostatic gating effect of the oxygen atoms in QC's. In both AC and QC molecular junctions, the conjugation is not broken and curly arrow rules works perfectly.

In contrast, in the junctions formed by AQ molecules, *meta* connected AQ2 shows a high conductance and constructive QI (blue curve in fig. 3e) whereas *para* connected AQ1 exhibits destructive QI with a low conductance (red curve in fig. 3e). This is opposite to the prediction using curly arrow rules, because when electrons are injected from site p in figure 3a,b, there is no electron path to the p' and p'' sites (fig. 3a,b) using curly arrow rules. Therefore, destructive QI is predicted from CARs, which is not supported with our calculation shown in figure 3e where AQ2 exhibits constructive QI. Similarly the *meta*-connected AQ2 shows constructive QI with high conductance, which is not consistent with predictions from curly arrow rules. This demonstrates that curly arrow rule breaks down in the *meta* connected anthraquinone.

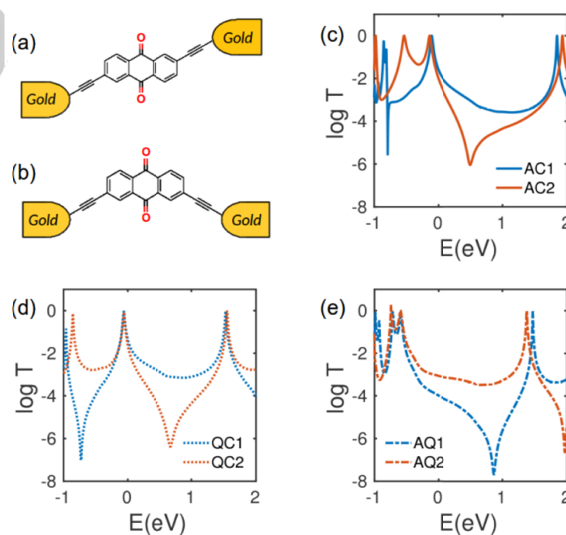


**Figure 4.** Transmission coefficients for electrons passing through the junctions with gold electrode through direct Au-C bond with acetylene linker. (a,b) example of junctions formed by AQ cores connected to the anchors from *para* and *meta* connectivities. Transmission coefficients for (c) AC1 and AC2, (d) QC1 and QC2 and (e) AQ1 and AQ2.

To demonstrate that this is a generic feature of anthraquinone-based molecular junctions, we study electron transport properties of the junctions formed from gold electrodes using either thiol or direct Au-C

anchor groups connected to AC, QC and AQ with *meta* or *para* connectivities. Figure 4 shows the transmission coefficient through the gold electrodes via direct Au-C coupling with acetylene linkers. Junctions formed with AC1 and QC1 molecular cores show constructive QI whereas those formed by AC2 and QC2 molecular core shows destructive QI (figs. 4c,d). The DFT Fermi energy lies in the tail of HOMO resonance in agreement with previous report<sup>[10]</sup> for molecular junctions formed through direct Au-C bond. Clearly, the destructive QI dip in QC2 has shifted to the right compared to AC2 due to the electrostatic gating effect of the oxygen atoms. The results for AC and QC are in agreement with predictions from curly arrow rules. However, the CAR again breaks down in the junctions formed by AQ molecular cores (fig. 4e), in agreement with our result obtained in graphene junctions (fig. 3). It is worth mentioning that although the transport is still HOMO dominated in the gold/AQ/gold junctions, the Fermi energy is closer to the middle of HOMO-LUMO gap.

We now consider a third system, where the three central cores are attached to gold electrodes through thiol anchors. Figure 5 shows the transmission coefficient obtained for these junctions. Clearly, the result is in excellent agreement with junctions formed from gold electrodes with Au-C direct anchoring (fig. 4) and graphene electrodes (fig. 3). Again, the conductance of the molecular junctions formed by both AC and QC molecular cores shows constructive and destructive interference for *para* and *meta* connectivities, respectively (figs. 5c,d) in contrast to the gold/AQ/gold junctions where opposite behavior is obtained (fig. 5e).

In order to understand the difference between the transmission coefficients of AQ and QC cores, we examined the evolution of the transmission coefficient starting from QC2 and then increasing the distances  $d$  between the hydrogens and oxygens of the two carbonyl groups in a series of steps. Fig. S11 shows that as  $d$  increases, the HOMO of QC2 evolves into the LUMO of AQ2 (see also figs S6 and S5), which pushes the anti-resonance from the HOMO-LUMO gap of QC2 into the LUMO-LUMO+1 gap of AQ2.

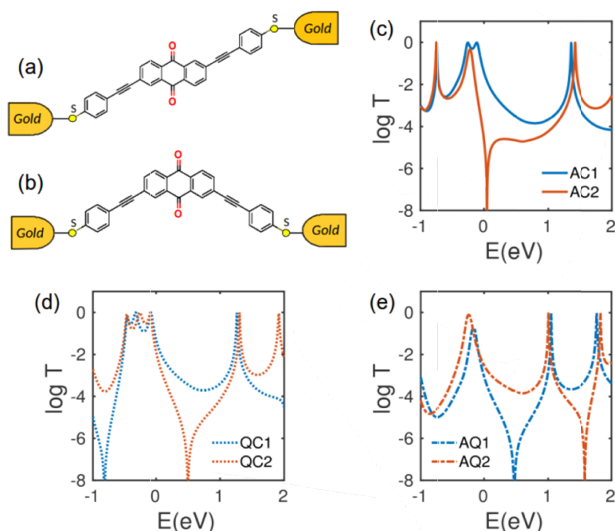


**Figure 5.** Transmission coefficients for electrons passing through the junctions with gold electrode with thiol anchor connected to thiol anchor. (a,b) example of junctions formed by AQ cores connected to the anchors from *para* and *meta* connectivities. Transmission coefficients for (c) AC1 and AC2, (d) QC1 and QC2 and (e) AQ1 and AQ2.

This surprising behavior in the AQ2 based junctions is also present in a simple tight-binding model of  $p$  orbitals within the molecules, in which the AC or AQ cores are connected to two 1D leads through a weak coupling (see methods). Figure 6 shows the calculate transmission coefficient  $T(E)$  for both *meta* and *para* connected junctions. Figure 6a shows  $T(E)$  for anthracene junctions with all on-site energies  $\epsilon_0=0$  and hopping integrals  $\gamma=-1$ . Clearly, constructive QI is obtained in the conjugated QC1 (AC1) junction compared to QC2 (AC2). When 9,10 ( $m$  and  $m'$  in the inset of figure 6a) hydrogen atoms in anthracene are replaced by oxygen, the on-site energies are increased due to electrostatic gating induced by oxygen atoms. This is captured by a minimal tight-binding model of cross-conjugated AQ junctions, where we only change the on-site energies at sites  $m$  and  $m'$  (see inset of fig. 6a) to  $\epsilon_m=\epsilon_{m'}=-1.5\gamma$ . This is because, in the cross conjugated structure, the site energy of carbon attached to an oxygen is increased. As shown by the resulting transmission coefficients in figure 6c, this leads to destructive QI for *para* connectivity and constructive QI for *meta* connectivity, in agreement with the  $T(E)$  of figure 5e, calculated from the material specific mean field DFT Hamiltonian.

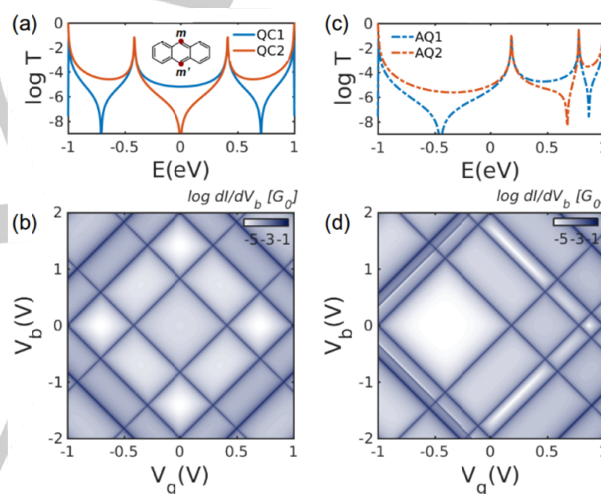


**Figure 6.** Simple tight-binding model. (a) the transmission coefficient for QC1 (blue line) and QC2 (red line). Inset (a) lattice structure considered in TB model. All on-site energies and couplings in a are  $\epsilon_0=0$  and  $\gamma=-1$ , respectively, (b) differential conductance of QC1 versus bias  $V_b$  and gate  $V_g$  voltages (c) the transmission coefficient for AQ1 (blue line) and AQ2 (red line) where all on-site energies and couplings in a are  $\epsilon_0=0$  and  $\gamma=-1$ , respectively; except on-site energies at sites  $m$  and  $m'$  ( $\epsilon_m=\epsilon_{m'}=-1.5\gamma$ ) and (b) differential conductance of AQ1 versus bias  $V_b$  and gate  $V_g$  voltages.

We also calculated the current through the junctions versus different bias  $V_b$  and gate  $V_g$  voltages using the method as discussed in ref<sup>[7]</sup>. By differentiating the current with respect to the bias voltage, we obtain the differential conductance  $G = dI/dV_b$ . In this model, we assume that the main bias potential drops at the interface between the leads and molecules and the gate voltage potential profile is uniform over the junctions. Figure 6b,d shows the calculated differential conductance for QC1 (AC1) and AQ1 junctions, respectively. The higher and lower conductances are illustrated by dark blue and white colours in figures 6b,d. By changing the redox state of QC1 to form AQ1, the conductance of the junction decreases by a couple of orders of magnitude due to the cross over from destructive (the diamond involving  $V_b=0V$  and  $V_g=0V$  in figure 6b) to constructive QI (the

diamond involving  $V_b=0V$  and  $V_g=0V$  in figure 6d). This opens new avenues for realization of quantum interference based single molecule switches.

In order to understand how interference patterns are affected by replacing oxygen atoms in AQ with two hydrogens to form broken conjugated dihydroanthracene (AH), we calculate the transmission coefficients for two *para* and *meta* connectivities attached to graphene or gold electrodes through either pi-pi stacking or using thiol or direct Au-C anchors. Figure S9 shows the transmission coefficient for these junctions. There is no signature of a strong destructive interference dip in these junctions in contrast with the destructive QI predicted by CARs. The transmission is slightly lower for *meta* connected junctions compared to *para* ones around DFT Fermi energy. Replacing hydrogens with methyl groups does not change the overall trends although the magnitude of differences between *meta* and *para* connectivities is generally more pronounced (fig. S10).

In summary, we demonstrated that curly arrow rules break down in molecular junctions formed by cross-conjugated anthraquinone. Curly arrow rules predict destructive QI for a *meta* connected anthraquinone core, whereas the first principle material specific calculation predicts constructive QI. This behavior is independent of choice of electrode material or anchor groups and arises from the evolution of the HOMO of dihydroxyanthracene into the LUMO of anthraquinone upon removal of the Hs from the pendant OH groups of dihydroxyanthracene. This pushes the anti-resonance from the HOMO-LUMO gap of *meta*-connected dihydroxyanthracene into the LUMO-LUMO+1 gap of *meta*-connected anthraquinone. In addition, we find that the destructive interference predicted by curly arrow rules in broken conjugated dihydroanthracene is not apparent in DFT-based transport calculations. Although, curly arrow rules are widely used by chemists, material scientists and engineers and have been successful in predicting destructive QI in many molecular junctions, it is not valid in cross-conjugated anthraquinone with *meta* connectivities to electrodes.

## Computational methods

The Hamiltonian of the structures described in this paper was obtained using DFT as described below or constructed from a simple tight-binding model with a single orbital per atom of site energy  $\epsilon_0=0$  and nearest-neighbor couplings  $\gamma=-1$ . On-site energies at sites  $m$  and  $m'$  (fig. 6a) are  $\epsilon_m=\epsilon_{m'}=-1.5\gamma$ .

**Density Functional Theory (DFT) Calculation.** The optimized geometry and ground-state Hamiltonian and overlap matrix elements of each structure were self-consistently obtained using the SIESTA<sup>[12]</sup> implementation of DFT. SIESTA employs norm-conserving pseudopotentials to account for the core electrons and linear combinations of atomic orbitals to construct the valence states. The generalized gradient approximation (GGA) of the exchange and correlation functional is used with the Perdew–Burke–Ernzerhof parameterization<sup>[15]</sup>, a double- $\zeta$  polarized basis set, a real-space grid defined with an equivalent energy cutoff of 250 Ry. The geometry optimization for each structure is performed for the forces smaller than 40 meV/Å.

**Transport calculation.** Transport Calculation. The mean-field Hamiltonian obtained from the converged DFT calculation or a simple tight-binding Hamiltonian was combined with Gollum<sup>[13]</sup> implementation of the nonequilibrium Green's function method to calculate the phase-

coherent, elastic scattering properties of the each system consist of left (source) and right (drain) leads and the scattering region. The transmission coefficient  $T(E)$  for electrons of energy  $E$  (passing from the source to the drain) is calculated via the relation  $T(E) = \text{trace}(\Gamma_R(E)G^R(E)\Gamma_L(E)E^{R\dagger}(E))$ . In this expression,  $\Gamma_{L,R}(E) = i(\Sigma_{L,R}(E) - \Sigma_{L,R}^\dagger(E))$  describes the level broadening due to the coupling between left (L) and right (R) electrodes and the central scattering region,  $\Sigma_{L,R}(E)$  are the retarded self-energies associated with this coupling, and  $G_R = (ES - H - \Sigma_L - \Sigma_R)^{-1}$  is the retarded Green's function, where  $H$  is the Hamiltonian and  $S$  is overlap matrix. Using the obtained transmission coefficient  $T(E)$ , the conductance could be calculated by the Landauer formula<sup>[16]</sup>  $G = G_0 \int dE T(E) \left(-\frac{\partial f}{\partial E}\right)$  where  $G_0 = 2e^2/h$  is the conductance quantum.

## Acknowledgements

H.S. acknowledges the Leverhulme Trust for Leverhulme Early Career Fellowship no. ECF-2017-186. Further support from the UK EPSRC is acknowledged, through grant nos. EP/M014452/1, EP/P027156/1, EP/N017188/1 and EP/N03337X/1.

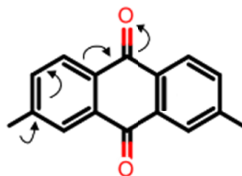
**Keywords:** Molecular Electronics • Quantum Interference • Curly Arrow Rules • Resonance-structure Analysis

- [1] a) S. V. Aradhya, L. Venkataraman, *Nat. Nanotechnol.* **2013**, *8*, 399–410; b) D. Xiang, X. Wang, C. Jia, T. Lee, X. Guo, *Chem. Rev.* **2016**, *116*, 4318–4440; c) T. A. Su, M. Neupane, M. L. Steigerwald, L. Venkataraman, C. Nuckolls, *Nat. Rev. Mater.* **2016**, *1*, 16002; d) M. Tsutsui, M. Taniguchi, *Sensors (Switzerland)* **2012**, *12*, 7259–7298.
- [2] a) R. Baer, D. Neuhauser, *J. Am. Chem. Soc.* **2002**, *124*, 4200–4201; b) S. H. Ke, Y. Weitaio, H. U. Baranger, *Nano Lett.* **2008**, *8*, 3257–3261; c) T. Markussen, R. Stadler, K. S. Thygesen, *Nano Lett.* **2010**, *10*, 4260–4265; d) H. Sadeghi, J. A. Mol, C. Siong, G. A. D. Briggs, J. Warner, C. J. Lambert, C. Lau, A. Briggs, J. Warner, C. J. Lambert, *Proc. Natl. Acad. Sci. USA* **2016**, *112*, 2658–63.
- [3] a) G. C. Solomon, D. Q. Andrews, R. H. Goldsmith, T. Hansen, M. R. Wasielewski, R. P. Van Duyne, M. A. Ratner, R. P. Van Duyne, M. A. Ratner, *J. Am. Chem. Soc.* **2008**, *130*, 17301–17308; b) C. M. Guédon, H. Valkenier, T. Markussen, K. S. Thygesen, J. C. Hummelen, S. J. Van Der Molen, S. J. Van Der Molen, *Nat. Nanotechnol.* **2012**, *7*, 305–309; c) F. Schwarz, E. Lörtscher, *J. Phys. Condens. Matter* **2014**, *26*, 474201.
- [4] W. O. Kermack, R. Robinson, *J. Chem. Soc., Trans.* **1922**, *121*, 427–440.
- [5] D. Z. Manrique, C. Huang, M. Baghernejad, X. Zhao, O. A. Al-Owaedi, H. Sadeghi, V. Kaliginedi, W. Hong, M. Gulcur, T. Wandlowski, et al., *Nat. Commun.* **2015**, *6*, 6389.
- [6] a) S. Sangtarash, C. Huang, H. Sadeghi, G. Sorohhov, J. Hauser, T. Wandlowski, W. Hong, S. Decurtins, S. X. Liu, C. J. Lambert, *J. Am. Chem. Soc.* **2015**, *137*, 11425–11431; b) Y. Geng, S. Sangtarash, C. Huang, H. Sadeghi, Y. Fu, W. Hong, T. Wandlowski, S. Decurtins, C. J. Lambert, S. X. Liu, *J. Am. Chem. Soc.* **2015**, *137*, 4469–4476; c) X. Liu, S. Sangtarash, D. Reber, D. Zhang, H. Sadeghi, J. Shi, Z. Y. Xiao, W. Hong, C. J. Lambert, S. X. Liu, *Angew. Chem. - Int. Ed.* **2017**, *56*, 173–176; d) S. Sangtarash, H. Sadeghi, C. J. Lambert, *Nanoscale* **2016**, *8*, 13199–13205; e) S. Sangtarash, H. Sadeghi, C. J. Lambert, *Phys. Chem. Chem. Phys.* **2018**, *20*, 9630–9637.
- [7] H. Sadeghi, *Nanotechnology* **2018**, *29*, 373001.
- [8] M. L. Perrin, R. Frisenda, M. Koole, J. S. Seldenthuis, J. A. C. Gil, H. Valkenier, J. C. Hummelen, N. Renaud, F. C. Grozema, J. M. Thijssen, et al., *Nat. Nanotechnol.* **2014**, *9*, 830–834.

- [9] P. Moreno-García, M. Gulcur, D. Z. Manrique, T. Pope, W. Hong, V. Kaliginedi, C. Huang, A. S. Batsanov, M. R. Bryce, C. Lambert, et al., *J. Am. Chem. Soc.* **2013**, *135*, 12228–12240.
- [10] Z. L. Cheng, R. Skouta, H. Vazquez, J. R. Widawsky, S. Schneebeli, W. Chen, M. S. Hybertsen, R. Breslow, L. Venkataraman, *Nat. Nanotechnol.* **2011**, *6*, 353–357.
- [11] H. Sadeghi, S. Sangtarash, C. Lambert, *Nano Lett.* **2017**, *17*, 4611–4618.
- [12] J. M. Soler, E. Artacho, J. D. Gale, A. García, J. Junquera, P. Ordejón, D. Sánchez-Portal, *J. Phys. Condens. Matter* **2002**, *14*, 2745–2779.
- [13] J. Ferrer, C. J. Lambert, V. M. García-Suárez, D. Z. Manrique, D. Visontai, L. Oroszlany, R. Rodríguez-Ferradás, I. Grace, S. W. D. Bailey, K. Gillemot, et al., *New J. Phys.* **2014**, *16*, 093029.
- [14] a) T. Markussen, J. Schiøtz, K. S. Thygesen, *J. Chem. Phys.* **2010**, *132*, 224104; b) H. Valkenier, C. M. Guédon, T. Markussen, K. S. Thygesen, S. J. van der Molen, J. C. Hummelen, *Phys. Chem. Chem. Phys.* **2014**, *16*, 653–662; c) D. Fracasso, H. Valkenier, J. C. Hummelen, G. C. Solomon, R. C. Chiechi, *J. Am. Chem. Soc.* **2011**, *133*, 9556–9563; d) J. P. Bergfield, H. M. Heitzer, C. Van Dyck, T. J. Marks, M. A. Ratner, *ACS Nano* **2015**, *9*, 6412–6418.
- [15] J. P. Perdew, K. Burke, M. Ernzerhof, *Phys. Rev. Lett.* **1996**, *77*, 3865–3868.
- [16] R. Landauer, *IBM J. Res. Dev.* **1957**, *1*, 223–231.

## COMMUNICATION

Curly arrow rules breakdown in molecular junctions formed by cross-conjugated anthraquinone. In contrast with the destructive quantum interference QI predicted by curly arrow rules for a meta connected anthraquinone core, we demonstrate that QI is constructive.



Jehan Alqahtani, Hatef Sadeghi,\* Sara Sangtarash, Colin J. Lambert

Page No. – Page No.

Breakdown of Curly Arrow Rules in Anthraquinone